*Journal of Nano- and Electronic Physics*
Vol. **17** No 5, 05018(6pp) (2025)

*Журнал нано- та електронної фізики*
Том **17** № 5, 05018(6cc) (2025)

OPEN ACCESS

**REGULAR ARTICLE**

# *p-i-n* Photodiode with a $p^+$ Guard Ring

D.O. Novikov[1,*], M.S. Kukurudziak[2,†], A.O. Voronko[1], M.S. Solodkyi[2], V.S. Antonyuk[1]

[1] *National Technical University of Ukraine "Igor Sikorsky Kyiv Polytechnic Institute", 03056 Kyiv, Ukraine*
[2] *Yuriy Fedkovych Chernivtsi National University, 5801, Chernivtsi, Ukraine*

(Received 12 September 2025; revised manuscript received 22 October 2025; published online 30 October 2025)

This paper presents the development and analysis of a silicon single-element *p-i-n* photodiode with a $p^+$-type guard ring that is isotopically identical to the substrate. The proposed structural solution facilitates the fabrication process, ensures better parameter stability, and reduces the effect of surface inversion channels on dark current and device sensitivity. The base material was high-resistivity (18 – 22 kΩ·cm), dislocation-free, monocrystalline p-type silicon with a <111> orientation. The device manufacturing process followed diffusion–planar technology, including consecutive formation of the $p^+$ guard ring and the $n^+$ light-sensitive region. Preliminary modeling of diffusion processes confirmed the absence of cross-doping between regions, revealed the dependence of dopant concentration profiles on depth, and also estimated the redistribution of dopant at the interface between materials during thermal-oxidative annealing and its subsequent changes during the diffusion stage. Measurements included both dark-current and photocurrent *I-V* characteristics, obtained at various wavelengths, in addition to the spectral response. The investigated photodiode demonstrated peak sensitivity around 950 – 970 nm with a quantum efficiency approaching 0.9, while at the YAG laser wavelength the QE was reduced to about 0.4. Full depletion of the space-charge region across the substrate thickness was observed at $U_{bias} = -100$ V. At this voltage, the signal rise and fall times saturate at their minimum values ($\tau_{rise} = 35 – 45$ ns, $\tau_{fall} = 40 – 45$ ns), with no additional reduction at higher biases. The results obtained emphasize the strong potential of the developed photodiode for practical implementation in optoelectronic devices. Its combination of high quantum efficiency, fast response time, and operational stability makes it suitable for laser detection, precision measurement, and telecommunication systems.

**Keywords**: Silicon photodiode, *p-i-n* diode, Doping, Dark current, Spectral response, Infrared detection.

DOI: 10.21272/jnep.17(5).05018 PACS numbers: 85.30. – z, 85.60.Dw, 07.57.Kp

## 1. INTRODUCTION

Widely used photodiodes (PDs) operating in photovoltaic mode are represented as PDs with $n^+$-$p$-$p^+$ -structure or *p-i-n* PDs [1]. In PDs with *p-i-n* structure, the *i*-region is located between two *n*-doped and *p*-doped regions and has a resistivity $10^6 – 10^9$ times greater than the resistivity of the doped regions. In *p-i-n* photodiodes, application of a sufficiently high reverse bias results in a strong electric field that extends through the entire intrinsic *i* region [2, 3]. Since this region can be designed quite wide, this type of structure creates the basis for a high-speed and highly sensitive PD. Silicon *p-i-n* photodiodes and coordinate-sensitive matrices based on them are widely used in various optoelectronic systems for receiving pulsed or modulated laser radiation in the spectral range of $\lambda = 0.4–1.1$ μm [4, 5].

The *p-i-n* PD design is realized using a high-resistance base material (usually *p*-type silicon) to ensure expansion of the space charge region over the entire *i*-region with a slight reverse bias [6]. A negative factor in the use of high-resistance *p*-type silicon is the formation of leading *n*-type inversion surface channels, which provoke a decrease in breakdown voltage [7], an increase in dark currents [8], a decrease in the insulation resistance of active multi-element PD elements or an increase in their photocoupling coefficient [9], as well as a decrease in sensitivity [10]. A constructive method for minimizing the influence of inversion layers on the PD parameters is the use of guard rings (GRs) of the same conductivity type as the sensitive elements ($n^+$-GR) [11-13]. Sometimes guard rings are implemented in combination with $p^+$-GR [14]. PDs with $n^+$-GR are usually used in samples with a high reverse bias voltage [2, 9]. When manufacturing low-voltage PDs, the formation of $n^+$-GR is impractical due to the need to additionally control the GR dark current, which significantly depends on the presence of inversion channels on the periphery of the crystal; the need to control the insulation resistance of the GR and sensitive elements with ensuring its high value (of the order of MΩ); the need

* Correspondence e-mail: d.novikov-me26@lll.kpi.ua
† mykola.kukurudzyak@gmail.com





Cite this article as: D.O. Novikov et al., *J. Nano- Electron. Phys.* 17 No 5, 05018 (2025) https://doi.org/10.21272/jnep.17(5).05018

to produce an additional terminal in the PD case for connecting the GR, etc. [9].

The fabrication of the photodiode with an isotype guard ring matched to the substrate material is recommended, which significantly simplifies the manufacturing technology and control of the final parameters of the devices. This paper will present the design features and development of low-voltage single-element silicon *p-i-n* photodiodes with $p^+$-GR, and will investigate their parameters, which will constitute the objective of this work.

## 2. EXPERIMENTAL SECTION

The study was conducted on silicon single-element *p-i-n* photodiodes with a responsive element (RE) area of $A_{RE} = 28$ mm$^2$ (Fig. 1), designed for detecting radiation from an Nd-doped YAG laser. The starting material was monocrystalline dislocation-free FZ-Si of *p*-type with [111] orientation, a resistivity $\rho \approx 18 - 22$ kΩ·cm, and a minority carrier lifetime $\tau \approx 1.9$ ms. Fabrication was carried out using diffusion-planar technology.

The technological process for fabricating photodiode consisted of the following steps: oxidation of the Si substrates using a dry-wet-dry oxidation sequence [15] at temperatures of 1403 – 1453 K; boron diffusion to form a guard ring isotype with the substrate material of $p^+$-type (acceptor concentration $N_A = 10^{18} - 10^{19}$ cm$^{-3}$); phosphorus diffusion (drive-in diffusion) into the front side of the substrate ($N_D \approx 10^{21}$ cm$^{-3}$) at $T = 1303 - 1353$ K to create $n^+$-type photosensitive elements; phosphorus redistribution in an oxygen atmosphere at 1403–1453 K to redistribute the dopant ($N_D \approx 10^{21}$ cm$^{-3}$), increase the depth of the $n^+$-$p$ junction, and grow a passivating $SiO_2$ layer with thickness optimized for minimum reflection of YAG laser radiation; boron diffusion into the backside of the substrate at 1203 – 1253 K ($N_A = 10^{19} - 10^{20}$ cm$^{-3}$) to passivate generation-recombination centers in the photodiode crystal bulk and form an ohmic $p^+$-layer; metallization and contact formation.

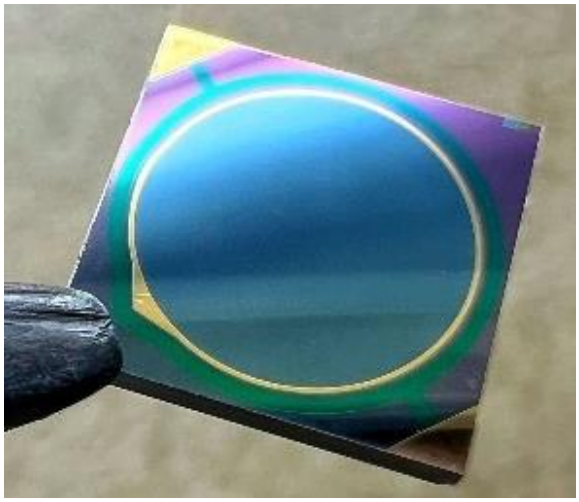

**Fig. 1** – Image of the photodiode crystal

### 2.1 Process Simulation in Technology Computer-Aided Design Environment

According to the proposed process flow, the structure illustrated in Fig. 2 was designed. Numerical simulations were subsequently performed to analyze the dopant distribution affected by segregation at the $Si/SiO_2$ interface during oxidation, together with the corresponding diffusion profiles, in order to evaluate and prevent cross-doping effects. The computational study was conducted using the Sentaurus simulation environment.

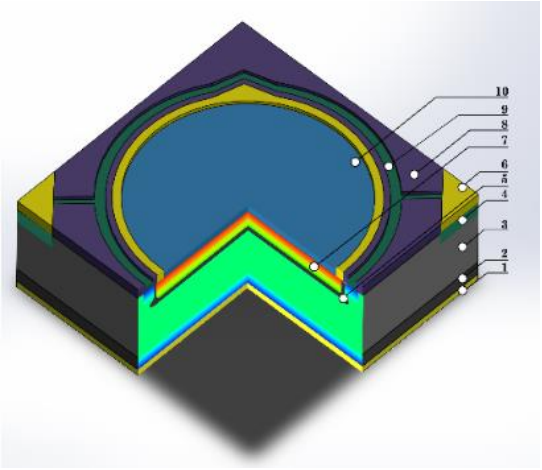


**Fig. 2** – Three-dimensional view of the simulated photodiode with a quarter cross-section illustrating the doping concentration gradients and structural elements: 1 — back-side metallization, 2 — boron-doped $p^+$-region, 3 — Si <111> substrate, 4 — $p^+$-guard ring region, 5 — space-charge region, 6 — front-side metallization, 7 — phosphorus-doped $n^+$-active region, 8 — protective oxide of the guard ring, 9 — protective oxide, 10 — antireflection oxide layer of the active region.

Analysis of the doping profiles of the front-side $n^+$-active region and $p^+$-GR (Fig. 3) allows the evaluation of doping concentration variations as a function of depth. The diffusion depth or phosphorus is about $X \approx 5.4$ μm, while for boron it is approximately $X \approx 5.8$ μm.

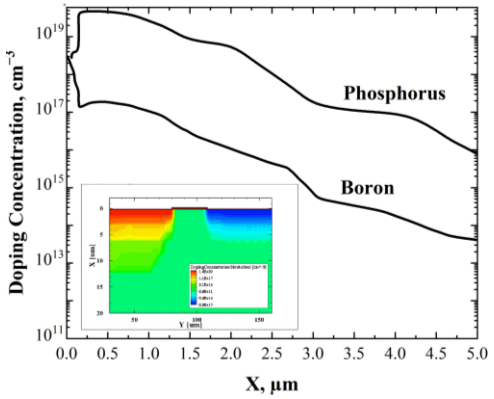


**Fig. 3** – Simulated doping concentration profiles of phosphorus and boron during diffusion

*p*-type impurities, including boron, gallium, and indium, tend to deplete from silicon, whereas *n*-type impurities, such as phosphorus, antimony, and arsenic, accumulate during thermal processing. The segregation coefficient of Boron decreases as the temperature rises and is greater for substrates with <111> orientation compared to those with <100> orientation. Boundary conditions were estimated by using the three-phase segregation model. During the simulation of oxide growth, the surface concentration of boron in the base region is seen to decrease (Fig. 4). As the segregation coefficient of boron is < 1 [16], boron atoms penetrate into the oxide, reducing the concentration at the surface. Consequently, this reduction can cause a reversal of surface conductivity polarity and initiate the formation of inversion layers.

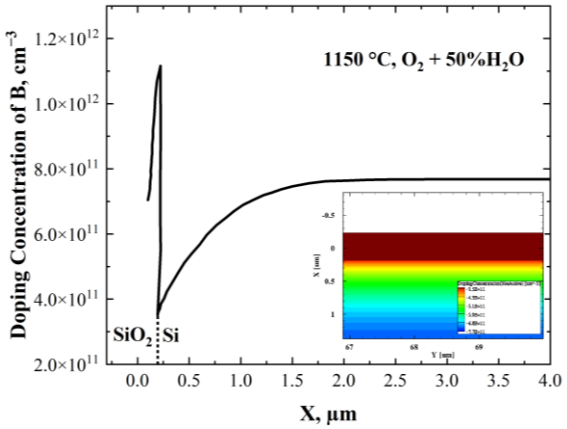


**Fig. 4** – Simulated change in surface concentration of boron during oxide layer growth

The $p^+$-type guard ring effectively suppresses the influence of surface inversion channels on the electrical characteristics of the photodiode, particularly the dark current, as the space-charge region of the photosensitive element under reverse bias is confined by the guard ring along the crystal surface.

### 2.2 Measurement Techniques

The *I–V* characteristics of the samples were obtained using an Arduino-based hardware-software complex, comprising an Agilent 34410A digital multimeter and a Siglent SPD3303X programmable power supply. Operation of the system was managed by a personal computer with software designed by the authors in the LabView environment. The current monochromatic pulse responsivity ($S_{pulse}$) was monitored at bias voltage $U_{bias}$ ranging from − 2 to – 100 V with a pulse duration $\tau_i = 500$ ns.

## 3. RESULTS AND DISCUSSION

From the dark current *I-V* characteristics of the investigated photodetectors (Fig. 5, inset), it can be seen that the dark current ($I_d$) increases with increasing reverse bias voltage as a result of the expansion of the space-charge region into the crystal bulk. As is well known, the dark current of a photodetector is determined by its bulk generation component and, accordingly, by the width of the space-charge region [18]:

$$I_d^G = e\frac{n_i}{2\tau}W_i A_{RE} \quad (1)$$

where $n_i$ is own concentration of charge carriers in the substrate; $e$ is the charge of the electron; $W_i$ is space charge region (SCR) width.

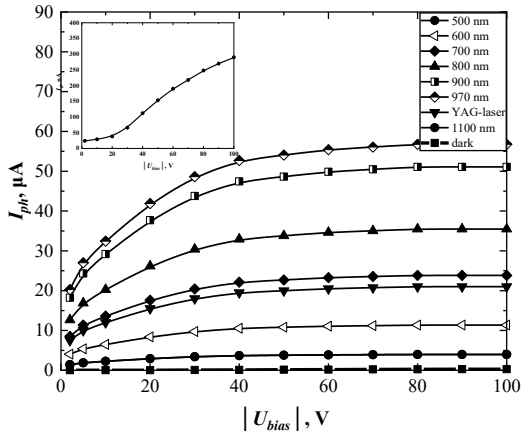


**Fig. 5** – *I–V* characteristics of the photodetectors under illumination at different wavelengths (inset: dark *I–V* characteristics)

The *I–V* characteristics of the photodetectors under illumination at different wavelengths were also obtained (Fig. 5), along with their corresponding spectral response (Fig. 6). It was found that the investigated sample exhibits peak sensitivity at wavelengths of 950 – 970 nm, with a quantum efficiency (QE) of approximately 0.9 in this range. At the YAG laser wavelength, the QE reaches about 0.4 (Fig. 6).

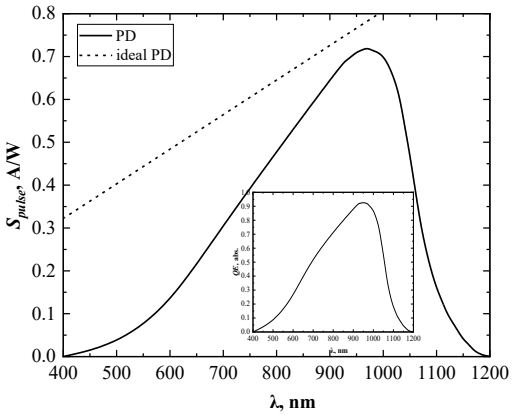


**Fig. 6** – Spectral sensitivity characteristic of the photodiode and its quantum efficiency

The short-wavelength minimum of the spectral response is determined by the depth of the *p–n* junction, which is 4 – 5 μm; accordingly, radiation with $\lambda \leq 400$ nm is absorbed by the doped layer [19]. The position of the short-wavelength edge of the spectral response can be adjusted by varying the depth of the phosphorus dopant. The long-

wavelength minimum of the spectral response is determined by the sensitivity of the bulk material, while the response close to 1000 nm depends on the crystal thickness together with the reflective properties of its back surface [20].

The dependence of $S_{pulse}$ on the bias voltage $U_{bias}$ was obtained (Fig. 7). It was found that at a bias voltage $U_{bias} = -90$ V, the photosensitivity reaches saturation, which indicates that the depletion region extends across the entire thickness of the substrate at this voltage.

In order to evaluate the photodetectors, their detectivity ($D^*$) was quantified using formula (2), and the dependence $D^*$ ($U_{bias}$) was obtained (Fig. 7 inset).

$$D^* = \sqrt{\frac{A_{RE}}{2eI}} S_{pulse} \tag{2}$$

From the dependence of $D^*$ ($U_{bias}$) it can be seen that within the voltage range of 0 – 20 V, there is a significant increase in detectivity due to a substantial rise in photosensitivity accompanied by a minimal change in dark current. As the voltage increases further, the dark current grows while the photosensitivity saturates, resulting in a decrease in detectivity. For $|U_{bias}| \geq 80$ V, the detectivity changes minimally because both the dark current and photosensitivity have reached saturation.

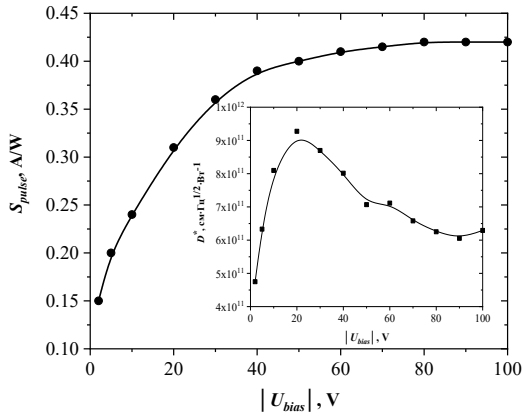


**Fig. 7** – Dependence of photodetector sensitivity on bias voltage

The output pulse characteristics of the photodetectors with a pulse duration of 500 ns were also measured. It was found that at the saturation voltage (Fig. 8a), i.e., when the space-charge region extends across the entire crystal thickness ($U_{bias} \approx -100$ V), the rise and fall times of the signal reach their minimum values and do not decrease further with increasing bias voltage ($\tau_{rise} = 35 - 45$ ns, $\tau_{fall} = 40 - 45$ ns). This behavior is due to the fact that in *p–i–n* photodetectors, the speed of response is dominated by carrier drift in the strong electric field; therefore, the highest speed is achieved when the space-charge region spans the full crystal thickness. At lower bias voltages, in addition to the drift component, a diffusion component appears because charge carriers are collected over a distance equal to the sum of the space-charge width and the diffusion length of minority carriers ($W_i + L_n$) from the *p–n* junction. The presence of the diffusion component in carrier transport to the *p–n* junction leads to a decrease in the detector speed ($U_{bias} \approx -80$ V), $\tau_{rise} = 90 - 100$ ns, $\tau_{fall} = 170 - 180$ ns).

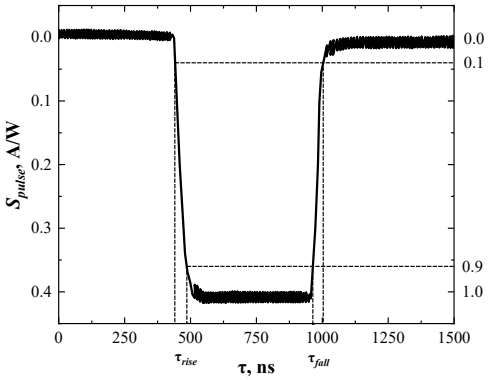


a

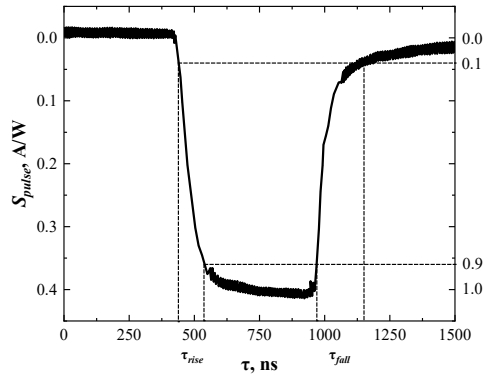


b

**Fig. 8** – Pulse output characteristics of PD at (a) $|U| = 100$ V and (b) $|U| = 80$ V

The electrons drift time $t_{dr}$ across the *i*-region of width *Wi* under an electric field *E* can be expressed as:

$$t_{dr} = \frac{W_i}{\nu_n} = \frac{W_i}{\mu_n E} \tag{3}$$

Here, $\nu_n = \mu_n E$ represents the electron drift velocity in an electric field E, and $\mu_n$ denotes the electron mobility. The ratio of the drift time across the *i*-region to the diffusion time through the *p–n* photodiode base $t_{dif}$ can be written as:

$$\frac{t_{dr}}{t_{dif}} = \frac{W_i / \mu_n E}{W_i^2 / 2D_n} = \frac{W_i^2 / \mu_n U_{bias}}{W_i^2 / 2D_n} = \frac{2\varphi}{U_{bias}} \tag{4}$$

As $D_n / \mu_n = kT / q = \varphi$, with $k$ as the Boltzmann constant and $T$ as the temperature.

It should be noted that the photodiode sensitivity reaches its maximum in two cases: when the space-charge region extends across the entire crystal thickness (5), or when the sum of the minority carrier diffusion length and the space-charge region width equals the crystal thickness (6).

$$X = L_n + W \tag{5}$$

$$X = W_i \tag{6}$$

Accordingly, by determining the thickness of the high-resistivity region of the photodetector crystal, the width of the SCR can be calculated using (6). Considering that the combined thickness of the phosphorus- and boron-doped layers is approximately 10 μm, and the total crystal thickness is 500 μm, the thickness of the high-resistivity *i*-region is 490 μm. Consequently, at a bias voltage of 100 V (saturation), the space-charge region extends to a thickness of 490 μm.

By knowing the thickness *Wi* of the high-resistivity region of the photodiode, the acceptor concentration $N_A$ in the $_i$-region can be calculated using formula (7):

$$W_i = \left( \frac{2\varepsilon\varepsilon_0(\phi_c - U_{bias})}{eN_A} \right)^{\frac{1}{2}} \tag{7}$$

Here, $\varepsilon$ and $\varepsilon_0$ denote the dielectric constants of silicon and vacuum, respectively, and $\varphi_c$ is the contact potential. Knowing the acceptor concentration and assuming full ionization of impurities at room temperature ($p = N_A$), the silicon resistivity can be calculated from the standard expression for *p*-type semiconductor conductivity:

$$\sigma = \frac{1}{\rho} = eN_A\mu_p \tag{8}$$

According to the applied methodology, it was found that the specific resistivity of the base material of the finished crystal reaches approximately $\rho = 20.5 - 21.5$ kΩ·cm, indicating minimal degradation of the silicon's electrophysical properties after processing. Maintaining a high specific resistivity of the crystal's *i*-region (and, correspondingly, a low doping concentration, $N_A$) allows fabrication of samples with minimal junction capacitance (Fig. 7), since the capacitance is inversely proportional to $N_A$ as:

$$C_{RE} = A_{RE} \left( \frac{\varepsilon\varepsilon_0 eN_A}{2(\phi_c - U_{bias})} \right)^{\frac{1}{2}} \tag{9}$$

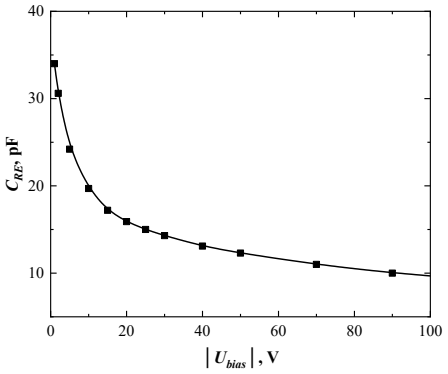


**Fig. 9** – Capacitance–voltage characteristics of the junction

## 4. CONCLUSIONS

A single-element silicon *p-i-n* photodiode incorporating a $p^+$-type guard ring isotopically consistent with the substrate material has been developed and fabricated. This design, comparable to structures with a $n^+$-type guard ring, demonstrates stable electrical characteristics by minimizing the influence of surface inversion channels. Utilization of high-resistivity silicon with a long minority-carrier lifetime ensures that dark current remains low while photosensitivity remains high. The high sensitivity is also attributed to the extension of the space-charge layer through the substrate at low voltages, thereby improving photogenerated carrier collection efficiency. Maximum spectral sensitivity was reached at 950 – 970 nm (QE ~ 0.9), while at the YAG laser wavelength the QE was about 0.4, confirming the photodiode's suitability for infrared detection. The results highlight the potential of the developed photodiode for future use in advanced optoelectronic applications, including laser detection systems, measurement instruments, and high-speed communication devices.

## AKNOWLEDGEMENTS

This work was conducted as part of the projects: (registration number 0125U000832, Rational design of quaternary detector materials for remote devices operating in conditions of significant radiation exposure, authors M.S. Kukurudziak and M.S. Solodkyi), (registration number 0125U001384, Experimental methods of optical pyrometry with emissivity compensation and deflectometry for measuring parameters of epitaxial semiconductor layers, authors A.O. Voronko and D.O. Novikov).

## REFERENCES

1. A. Chierici, R. Ciolini, D.S. Nascimento, F. d'Errico, *Radiat. Meas.* **177**, 107258 (2024).
2. F. Alghannam, N.S. Alharthi, M. Alayed, *Front. Phys.* **13**, 1563838 (2025).
3. Z. Wei, J. Yu, M. Zuo, P. Nie, *J. Appl. Phys.* **135**, 114502 (2024).
4. V.G. Verbitskiy, V.S. Antonyuk, A.O. Voronko, L.M. Korolevych, D.O. Verbitskiy, D.O. Novikov, *J. Nano- Electron. Phys.* **13** No 4, 04026 (2021).
5. K. Schneider-Hornstein, B. Goll, H. Zimmermann, *IEEE Photon. J.* **15**, 6801009 (2023).
6. H. Liu, T.P. Pasanen, T.H. Fung, J. Isometsä, A. Haarahiltunen, S. Hesse, H. Savin, *Light Sci. Appl.* **14**, 9 (2025).

7. F. Rezaei, N. Dehghan, F. Rezaeian, *IET Circuits Devices Syst.* **16**, 491 (2022).
8. L. Yao, Z. Zhou, Y. Zhu, Y. Rao, Y. Hu, C. Li, S. Chen, *IEEE Trans. Electron Dev.* **71**, 3921 (2024).
9. M.S. Kukurudziak, *J. Instrum.* **19**, P09006 (2024).
10. A. Bablich, M. Müller, R. Bornemann, A. Nachtigal, P.H. Bolívar, *Photon. Sens.* **13**, 230415 (2023).
11. S. Hoque, M.A. Abdullah, M. Alayed, M. Elamien, M.J. Deen, *IEEE Electron Device Rev.* **3**, 50 (2025).
12. D. Khaled, S. Rugen, N. Kaminski, H. Umezawa, H. Okumura, E. Gheeraert, *Diam. Relat. Mater.* **82**, 160 (2018).
13. M. Mekheldi, S. Oussalah, A. Lounis, N. Brihi, *J. Nano-Electron. Phys.* **11** No 4, 04008 (2019).
14. Z. Ebrahimi, B. Gosselin, *IEEE Sens. J.* **24**, 11123 (2024).
15. S.W. Glunz, F. Feldmann, *Sol. Energy Mater. Sol. C.* **185**, 260 (2018).
16. H. Chen, K. Morita, X. Ma, Z. Chen, Y. Wang, *Sol. Energy Mater. Sol. C.* **203**, 110169 (2019).
17. H.P. Parkhomenko, M.M. Solovan, A.I. Mostovyi, I.G. Orletskyi, V.V. Brus, *Eur. J. Phys.* **4**, 43 (2021).
18. K.V. Ravi, *Imperfections and Impurities in Semiconductor Silicon* (Wiley, New York, 1981).
19. M.S. Kukurudziak, E.V. Maistruk, *East Eur. J. Phys.* **1**, 386 (2024).
20. A. Voronko, D. Novikov, O. Shymanovskyi, *Radioelectron. Commun. Syst.* **66**, 74 (2024).


## *p-i-n* фотодіод із захисним кільцем $p^+$


Д.О. Новіков[1], М.С. Кукурудзяк[2], А.О. Воронько[1], М.С. Солодкий[2], В.С. Антонюк[1]

[1] *Національний технічний університет України "Київський політехнічний інститут імені Ігоря Сікорського", 03056 Київ, Україна*

[2] *Чернівецький національний університет імені Юрія Федьковича, 58012 Чернівці, Україна*



В даній роботі представлено розробку та аналіз одноелементного кремнієвого *p-i-n* фотодіода з охоронним кільцем $p^+$-типу, ізотопно подібним до підкладки. Запропоноване конструктивне рішення спрощує процес виготовлення, забезпечує кращу стабільність параметрів і зменшує вплив поверхневих інверсійних каналів на темновий струм та чутливість приладу. Вихідним матеріалом був монокристалічний кремній *p*-типу з орієнтацією <111>, високого питомого опору (18 – 22 кΩ·см), без дислокацій. Технологія виготовлення приладу ґрунтувалася на дифузійно-планарному процесі й включала послідовне формування охоронного $p^+$ кільця та світлочутливої $n^+$ області. Попереднє моделювання дифузійних процесів підтвердило відсутність перехресного легування між областями, виявило залежність профілів концентрації домішок від глибини, а також дозволило оцінити перерозподіл домішки на межі розділу матеріалів під час термічного окиснення та його подальші зміни на стадії дифузії. Експериментальні дослідження включали вимірювання ВАХ темнового струму та фотоструму при різних довжинах хвиль, а також визначення спектральної чутливості. Досліджуваний фотодіод продемонстрував пікову чутливість у діапазоні 950 – 970 нм із квантовою ефективністю (QE), значення якої наближається до 0.9, тоді як на довжині хвилі YAG-лазера значення QE зменшилося приблизно до 0.4. Повне збіднення області просторового заряду по всій товщині підкладки спостерігалося при $U_{bias} = -100$ В. За цієї напруги часи наростання та спаду сигналу насичувалися на мінімальних значеннях ($\tau_{rise} = 35 – 45$ нс, $\tau_{fall} = 40 – 45$ нс) без подальшого зменшення при більших напругах зміщеннях. Отримані дані підтверджують високий потенціал фотодіода для впровадження в оптоелектронних системах. Поєднання високої квантової ефективності, малої тривалості відгуку та стабільності параметрів робить його перспективним для застосування у сфері лазерного детектування, високоточного вимірювання та телекомунікацій.



**Ключові слова:** Кремнієвий фотодіод, *p-i-n* діод, Легування, Темновий струм, Спектральна чутливість, Детектування інфрачервоного випромінювання.